Terrain Reconstruction of Glacial Surfaces via Robotic Surveying Techniques

Stephen Williams, Lonnie T. Parker, and Ayanna M. Howard

***Abstract*—The capability to monitor natural phenomena using mobile sensing is a benefit to the Earth science community given the potentially large impact that we, as humans, can have on naturally occurring processes. Observable phenomena that fall into this category of interest range from static to dynamic in both time and space (i.e. temperature, humidity, and elevation). Such phenomena can be readily monitored using networks of mobile sensor nodes that are tasked to regions of interest by scientists. In our work, we hone in on a very specific domain, elevation changes in glacial surfaces, to demonstrate a concept applicable to any spatially distributed phenomena. Our work leverages the sensing of a vision-based SLAM odometry system and the design of robotic surveying navigation rules to reconstruct scientific areas of interest, with the goal of monitoring elevation changes in glacial regions. We validate the output from our methodology and provide results that show the reconstructed terrain error complies with acceptable mapping standards found in the scientific community.**

THE ability to understand the causes and effects of climate change is one of the foremost questions under consideration in the scientific community today. Since the 1970s, scientists have gathered weather-related measurements from around the globe to study this phenomenon and begin to model the major contributing factors as well as predict the global ramifications. It has been discovered that the world's glacial regions are particularly sensitive to changes in the climate; the dwindling ice caps are but one sign of this region's increasing temperatures [1], [2]. Due to the sensitivity of these regions, scientists have focused data gathering efforts towards the poles, setting up networks of automatic weather stations in Greenland and Antarctica [3], [4]. These stations are expensive to install and maintain, yet provide only sparse spatial resolution in these critical areas. To augment the data collection mechanisms available to climate scientists in harsh, glacial terrain, a multi-agent robotic sensor network has been proposed [5]. The network would consist of multiple autonomous robotic rovers equipped with a customizable sensor payload. The scientists would define the region of interest and desired spacial resolution, then task the network to execute the data-gathering mission.

The multi-agent nature of the proposed system poses certain design constraints. Most notably, because the system will consist of many robotic nodes, each node must be minimally expensive. This pushes the design away from centimeter accuracy GPS units and military-grade IMUs and towards consumer-grade sensing equipment. Consumer-grade sensing, however, generally does not have the localization accuracy necessary for the positioning of the robotic nodes into the requested sampling topology. Consumer-grade sensors must therefore be augmented with other real-time measurements to create a higher-accuracy localization system.

For efficient traversal to the designated location, each robotic node must plan a safe and efficient path through the terrain. While the algorithms employed by global path planners differ significantly, from the dynamic programming methods of Dijkstra's algorithm [6] to the random sampling methods of rapidly-exploring random trees [7], all planning strategies require a map on which to plan. Coarse scale maps are generally available from remote sensing technologies. However, at typical resolutions greater than 100 meters [8], these maps are unable to capture rover-scale terrain structures, which could impede travel or affect the accuracy of derived scientific measurements. Additionally, glacial terrain is often dynamic in nature, with snow dunes changing shape and location over time and new cracks forming in the ice surface. In order for the planned paths to be useful, the course-scale terrain map must be augmented with local-scale features encountered by the robotic platform during the traverse. Ideally, the terrain should be sensed or predicted before the platform encounters these obstacles, allowing new paths to be planned as far in advance as possible.

In addition to improving navigational performance, the terrain reconstruction itself can be a key scientific data product. For example, climate researchers have been studying the ice mass balance of glacial systems. By monitoring the relative elevation changes of the glacier surface, they can estimate the change in ice volume. Currently, scientists install ablation wires at key points in the glacier surface or use relative elevation readings from automatic weather stations. However, these single-point measurement strategies must interpolate over large areas to estimate ice mass balance values [9]. A much more accurate assessment of ice mass balance could be obtained if the glacial surface were periodically surveyed. In such a scenario, the robotic agents could be tasked to survey the glacial surface with the goal of creating a terrain reconstruction meeting certain error criteria. However, if the main purpose of rover mission is to perform a glacier survey, a different set of path planning strategies are required.

In the following sections, a vision-based simultaneous localization and mapping (SLAM) algorithm is described that was tailored to meet the challenges of using vision systems in low-contrast, glacial environments. As a by-product of calculating the robot's pose estimate, the SLAM system also estimates the positions of a large number of terrain landmark points. An adaptive terrain reconstruction methodology is proposed that creates a topographic terrain map using these vision-based terrain measurements as input. Additionally, prior terrain knowledge, such as course-scale satellite elevation

measurements, can be incorporated into the terrain model in a natural way, further improving the reconstruction quality. This is originally motivated by the need for forward-looking maps for path planning algorithms. However, once the focus changes to "maps as the end product," different planning mechanisms are needed. Several surveying strategies are discussed, as well as methods for selecting the surveying path parameters based on prior knowledge of the terrain and guided by common mapping standards. We also introduce the concept of science-centric coverage to better evaluate the meaning of collected science information as it relates to the surveying strategies. Both the vision-based terrain sampling methods and the described surveying path planners are validated within a simulation environment created to mimic a glacier field test site.

I. Robotic Sensor Network

Previous arctic robotics projects, such as Nomad out of CMU [10], [11] and MARVIN from the University of Kansas [12], [13], showcase the ability of the mechanics of a robot to survive the inhospitable climate of glacial environments. However, each of these projects involves the construction of a single, expensive robotic agent. Such an approach is not practical for the development of multi-agent systems, where potentially dozens of robotic agents will be utilized.

Instead, each agent must cope with low-cost, commodity sensors. However, consumer-grade GPS receivers and IMUs do not have the localization accuracy necessary for the positioning of the robotic nodes into the request sampling topology. These sensors must be augmented with additional information to produce a viable system. In particular, vision is an attractive option. It is the sensing modality relied upon most by humans, and it has been shown effective for both the Mars rovers [14] and DARPA Grand Challenge vehicles [15]. Compared with laser scanners, even high resolution cameras are light, low power, and inexpensive.

A. Vision System

To augment the GPS localization system, a vision-based simultaneous localization and mapping (SLAM) algorithm has been implemented. Vision-based SLAM systems seek to estimate the 3D pose of the camera by tracking the coordinates of visually distinct features in the environment. As the features move in image space, the relative motion is used to update the position of the camera, as well as estimate the 3D location of the features themselves. This requires that images features be reliably extracted and matched within the image stream. One of a number of common keypoint detectors are generally used to meet the feature detection needs, such as Harris [16] or SIFT [17]. These detectors rely on finding pixels with strong directional gradients. However, glacial environments generally lack these types of distinctive features.

Since standard feature detectors search for pixels exhibiting strong directional gradients, the foreground image gradient must be boosted for these detectors to perform properly. Ideally, the image enhancement should be non-uniform, adaptively enhancing the foreground regions while leaving areas of sufficient contrast alone. A contrast-limited adaptive histogram equalization preprocessing stage has been shown to drastically improve both the detection rate and matching consistency of standard feature detectors when applied to low-contrast, glacial scenes [18]. This allows standard visual SLAM techniques to be applied in the domain of glacial robotics.

However, SLAM systems are incremental, with the current position estimate updated based on a change in observations. One of the fundamental issues when using any incremental localization system is drift. As the system runs, small errors accumulate, resulting in significant localization error over time. The final localization system thus uses a particle filter to fuse the low-quality GPS measurements with the incremental localization of visual SLAM, producing a system capable of both consistent local-scale localization and drift-free global-scale positioning. Using this fused approach, typical accuracies of less than $1.0m$ were possible on field trial data collected on Mendenhall Glacier near Juneau, Alaska [19].

B. Robotic Platform

Additionally, high terrain mobility is required for testing and proper execution of science missions. While much of the rover's time will be spent in the flat, central regions of the glacier, the project goal is to construct a system capable of traversing the widest range of expected terrain possible. Typically the areas of most interest to scientists occur at the extremes of the environment. Collecting data about a forming glacial lake requires descending into the surrounding basin as shown in Figure 1, while investigating the glacier-mountain boundary requires ascending steep slopes.

For these reasons a snowmobile chassis was selected as the base for the SnoMote prototype robotic mobile sensor [20]. The chassis, based on an RC snowmobile chassis, was heavily modified to incorporate a dual-track design. The modified platform has been equipped with an on-board embedded computer, consumer-grade GPS unit for global localization, and a wide-angle monocular camera for real-time image processing. Only a minimal amount of sensing was incorporated into the rover design to test the extents to which the vision system could supply the situational awareness and terrain assessment needs of the mobile rover.

To simulate the science objectives, a weather-oriented sensor suite was added to the rover. Ultimately, the science package will include an extensive set of weather-related equipment, such as an anemometer or solar radiation sensor. For prototyping, a set of solid-state sensors were selected that could measure meaningful weather related data and still fit within the confines of the rover's chassis. The final instrument suite includes sensors to measure temperature, barometric pressure, and relative humidity. Figure 2 shows a diagram of the prototype robotic platform.

II. Vision-based Terrain Reconstruction

In order for each robotic agent to achieve its goal location within the sensor network, a path plan must be generated that keeps the rover on safe, traversable terrain. However, before such a plan can be generated, an appropriate map is required

Fig. 1. The SnoMote Mk2 prototype rover descending into a glacial lake basin.

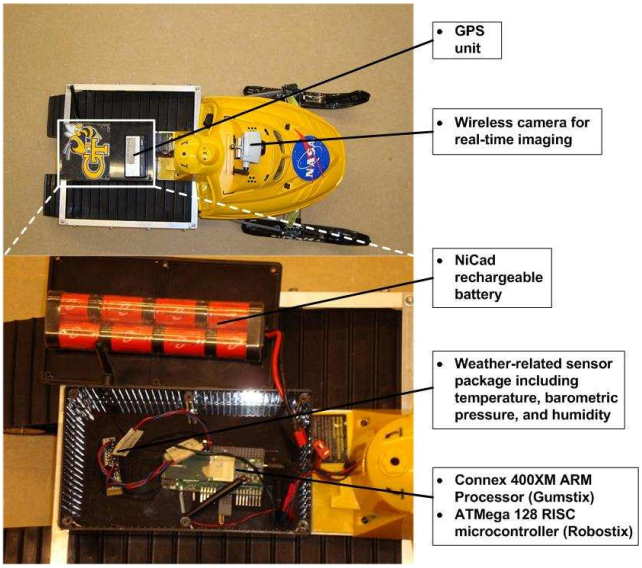

Fig. 2. A diagram of the major components of the SnoMote Mk2 prototype robotic weather station network node.

(a) Mendenhall Glacier Field Trial Site

(b) Gazebo Simulation

Fig. 3. Examples of dynamic terrain hazards encountered during field trials in glacial environments. (a) a large crevasse, (b) exposed ice with irregular surface and melt-water pools.

that captures the types of terrain obstacles present in a given environment at a scale similar to that of the rover. Specifically, the major obstacles in glacial environments are slope based [21], [22], making knowledge of the rover's orientation in the environment important when determining traversability. Hence, a topographic map is a natural choice, allowing the planning algorithm to predict the rover orientation over the entire path. However, an up to date topographic map with an appropriate scale is difficult to obtain.

Recently satellite missions such as the Shuttle Radar Topography Mission (SRTM) [23] and NASA's Ice, Cloud, and land Elevation (ICESat) satellite [24] have mapped the globe with increasing accuracy. However, even the best of these satellite-generated digital elevation models (DEMs) has a minimum resolution far greater than the scale of the robotic platform. When combined with the dynamic nature of glacial environments (snow dunes change shape and location over time and new cracks form in the ice surface, examples of which are shown in Figure 3), it is impossible for these types of maps to capture all the hazards a rover might encounter during a mission.

A second source of available mapping information comes from the augmented localization system. The SLAM algorithm produces a set of 3D landmarks on the terrain surface as a byproduct of estimating the rover's pose. However, the terrain slope is an important aspect in the planning strategy, something not immediately available from a set of sparse 3D points. Additionally, SLAM landmarks are localized incrementally by viewing the landmark with increasing amounts of parallax. This means that the most accurate landmark positions will be obtained as the rover passes by the landmark position, and landmarks that are directly in front of the rover will retain large amounts of uncertainty. This has detrimental implications for use in path planning, where the terrain structure in front of the rover is of far more interest than the terrain behind.

A terrain reconstruction method is presented that uses the sparse landmark position estimates from the localization system as input to a statistical interpolation system known

as a Gaussian process (GP). A GP intrinsically handles measurement uncertainty, allowing the calculation of both the maximally likely terrain surface and the terrain uncertainty. Additionally, the GP uses information about observed terrain to predict unobserved terrain, albeit with increasing levels of uncertainty. This obviates the issues with using SLAM landmarks directly. Additionally, the GP can incorporate *a priori* knowledge of the terrain structure through the use of a mean function. The predicted terrain is then pulled away from the mean in response to measurements of the real terrain. This allows the course satellite data to bootstrap the reconstruction system while providing a mechanism for correcting and augmenting this information due to conditions on the ground.

A. Gaussian Processes

A Gaussian process (GP) is a collection of an infinite number of random variables with a jointly Gaussian distribution [25]. This may be interpreted as a distribution over continuous functions, similar to how a Gaussian variable defines a distribution over real values. Instead of sampling a value in $\mathbb{R}^N$ from the Gaussian variable, a continuous function, $f(\vec{x})$, is drawn from the GP that maps an input vector, $\vec{x} \in \mathbb{R}^N$, to an output value, $y \in \mathbb{R}$. A GP is defined by a mean function, $\mu(\vec{x})$, which describes the mean output value of all possible sample functions evaluated at the input, $\vec{x}$, and a covariance function, $k(f(\vec{x}_i), f(\vec{x}_j))$, which describes the correlation between any pair of output values. The choice of the mean and covariance functions allows prior knowledge of the function's behavior to be encoded in the GP framework. While many covariance functions are possible, a common and natural choice is the squared exponential function listed in Equation (1). This covariance function is derived from a Gaussian kernel, exhibits rotation and translation invariance to the inputs, and is infinitely differentiable or infinitely smooth. The exact spatial behavior of the covariance function can be tuned with a function-dependent set of parameters, known as hyperparameters in GP literature [25].

$$k\left(f(\vec{x}_i), f(\vec{x}_j)\right) = \alpha \exp\left(-\frac{1}{2}\left(\vec{x}_i - \vec{x}_j\right)^T \Gamma \left(\vec{x}_i - \vec{x}_j\right)\right) \quad (1)$$

where Γ is a diagonal matrix of elements $\frac{1}{\gamma_1}, \ldots, \frac{1}{\gamma_N}$, and α is a scaling factor. The variables in the $N+1$ dimensional set $\alpha, \gamma_1, \ldots, \gamma_N$ are known as the hyperparameters for the squared exponential Gaussian process.

To draw a sample, the GP must be evaluated at each input value, $\vec{x}$. However, as stated previously, a GP is an infinite dimensional object. Despite the infinite dimensional nature of GPs, sampling is still computationally tractable due to the marginalization property. If a GP is defined over a set, S, by $\mathcal{GP}(\mu, \Sigma)$, then the GP is also defined over any subset of S by the relevant submatrices of μ and Σ, as shown in Equation (2). Thus, as long as the number points at which $f(\vec{x})$ is to be evaluated is finite, then sampling from the GP is also finite. Equivalently, any finite set of variables from a GP have a jointly Gaussian distribution [25].

$$p(y_i, y_j) \sim \mathcal{N}\left(\begin{bmatrix}\mu_i \\ \mu_j\end{bmatrix}, \begin{bmatrix}\Sigma_{i,i} & \Sigma_{i,j} \\ \Sigma_{j,i} & \Sigma_{j,j}\end{bmatrix}\right) \Rightarrow p(y_i) \sim \mathcal{N}\left(\mu_i, \Sigma_{i,i}\right) \quad (2)$$

A GP can also be conditioned on a set of known measurements [25]. The resulting GP posterior describes only the subset of sample functions that pass through the measurement points. This allows the GP to be used as a regression or interpolation technique, in which samples may be queried at an arbitrarily small resolution. However, unlike conventional regression or interpolation techniques, no data model (linear, quadratic, etc.) is required. For interpolation, a set of unknown output values, $Y^* = \left\{y_j^* | j = 1, \ldots, Q\right\}$, is desired, corresponding to a set of known inputs values, $X^* = \left\{\vec{x}_j^*\right\}$. The output values are to be conditioned on a set of known measurements, $Y = \{y_i | i = 1, \ldots, P\}$, corresponding to a second set of known input values, $X = \{\vec{x}_i\}$. The GP posterior mean and covariance satisfying these conditions are shown in Equation (4) and (5) (with a full derivation available in [26]).

$$p(Y^* | X, Y, X^*) \sim \mathcal{N}\left(\mu^*, \Sigma^*\right) \quad (3)$$

$$\mu^* = \mu_X + \Sigma_{Y,Y^*} \cdot \Sigma_{Y^*,Y^*}^{-1} \cdot (Y - \mu_X) \quad (4)$$

$$\Sigma^* = \Sigma_{Y,Y} - \Sigma_{Y,Y^*} \cdot \Sigma_{Y^*,Y^*}^{-1} \cdot \Sigma_{Y,Y^*}^T \quad (5)$$

where μ_S is a vector of values produced by evaluating the mean function, $\mu(\cdot)$, over the set, S, and Σ_{S_1,S_2} is a covariance matrix constructed by evaluating the covariance function, $k(\cdot,\cdot)$, with each pair-wise combination of values from sets S_1 and S_2.

B. Visual Landmarks

A Gaussian Process (GP) terrain model is capable of combining multiple measurements of the terrain elevation into a single, cohesive representation. The GP model also incorporates any measurement uncertainty into the reconstruction, if that uncertainty may be modeled by additive independent Gaussian noise. In that case, the measurement covariance matrix, $\Sigma_{Y,Y}$, is simply augmented by the elevation uncertainty of each measurement, as in Equation (6). Geostatistical models often use GPS survey data collected in a uniform grid or other sampling technique designed to capture the observed terrain variation. The positional errors associated with GPS survey data tend to be small and relatively uncorrelated, making this a good fit for GP interpolation.

$$\Sigma'_{Y,Y} = \Sigma_{Y,Y} + \begin{bmatrix}\sigma_1^2 & & \\ & \ddots & \\ & & \sigma_N^2\end{bmatrix} \quad (6)$$

where σ_i^2 is the elevation variance of the i^{th} measurement.

The visual SLAM algorithm within the localization system produces a set of 3D point estimates that lie on the terrain surface as a byproduct of the localization process, superficially analogous to GPS data. However, unlike GPS surveys, this data is collected opportunistically while the robot performs a

traverse, rather than with the explicit goal of capturing terrain variations. These visual landmarks also cover the terrain only sparsely, with landmarks near the rover's path occurring far more frequently than landmarks at significant distances. While this may be suboptimal from a terrain sampling standpoint, no additional travel is incurred by the rover to collect this data.

Further, the uncertainty of each SLAM landmark is a jointly Gaussian distribution in both the dependent variables, (x, y), and the independent variable, z. Inclusion of uncertainty in the dependent variables is known as the "error-in-variables" problem in statistics, and few solutions exist for the multivariate case [27]. Rather than attempting to modify the GP structure to incorporate "error-in-variables" uncertainty, each landmark covariance is converted into independent additive noise by marginalizing out the dependent variables, (x, y), from the joint distribution, as shown in Equation (7). Due to the highly directional nature of visual SLAM landmark estimates, removing the dependency of x and y, even from covariances with even a small volume, results in a large elevation uncertainty. For this reason, only those landmark estimates whose depth uncertainty have collapsed to a small region are considered for inclusion in the GP terrain reconstruction.

$$\begin{aligned} p(z) &= \int_x \int_y p(x, y, z)\, dx\, dy \\ &= \int_x \int_y \mathcal{N}\left(\begin{bmatrix} \mu_x \\ \mu y \\ \mu_z \end{bmatrix}, \begin{bmatrix} \sigma_x^2 & \alpha\sigma_x\sigma_y & \beta\sigma_x\sigma_z \\ \alpha\sigma_y\sigma_x & \sigma_y^2 & \gamma\sigma_y\sigma_z \\ \beta\sigma_z\sigma x & \gamma\sigma_z\sigma_y & \sigma_z^2 \end{bmatrix} \right) dx\, dy \\ &= \mathcal{N}\left(\mu_z, \sigma_z^2\right) \end{aligned} \tag{7}$$

C. Satellite Elevation Data

DEMs produced by satellite missions such as SRTM or ICESat average the terrain elevation over a large area compared with the size of the rover. While this information cannot capture the local-scale hazards faced by the robotic sensor node, it can serve as an indication of large-scale terrain variations. Within the GP framework, a mean function, $\mu(\vec{x})$, is specified. This is typically set to a constant value, calculated from the mean of all the observation values. The GP then models the terrain deviation from the mean. However, if a better terrain elevation expectation is available, this can be easily incorporated into the GP instead. In particular, while it is referred to as a mean function, it need not be written in analytical form. It simply must be evaluable at the measurement locations, X, and the query locations, X^*. This can easily be accommodated using simpler interpolation methods on the satellite data, or even from an online mapping service such as U.S. Geological Survey [28] or Google Earth.

D. Hyperparameter Optimization

The GP framework is considered a model-free regression technique in that no functional model, such as a linear or logarithmic function, is used during the data fit. However, the behavior of the GP can be tuned to a specific problem through the use of the covariance function hyperparameters. In Equation (1), the terms $\alpha, \gamma_1, \ldots, \gamma_N$ are known as the hyperparameters for the squared exponential Gaussian process. The values γ_i are often referred to as the length scales. The distance between the input variables in each dimension is divided by the corresponding length scale value during the covariance calculation. This allows the GP to vary how quickly the output can change in response to the inputs. In terrain modeling, length scales in the tens to hundreds of meters are common. The α parameter is a gain value placed on the entire covariance function. This allows the GP model to be more or less sensitive to the input values as a whole.

The hyperparameters for a GP model are ideally trained on a subset of data to maximize the posterior probability shown in Equation (8). However, if no prior probability information is known for the hyperparameter distribution, $p(\theta)$, then the common practice of maximizing the log marginal likelihood, $log\left(p(Y|X, \theta)\right)$, is equivalent. The log marginal likelihood for a GP is shown in Equation (9) [29].

$$p\left(\theta|X, Y\right) = \frac{p\left(Y|X, \theta\right)\ p\left(\theta\right)}{p\left(Y|X\right)} \tag{8}$$

$$\log\left(p\left(Y|X, \theta\right)\right) = -\frac{1}{2} Y^T\, \Sigma_{Y,Y}^{-1}\, Y - \frac{1}{2} \log|\Sigma_{Y,Y}| - \frac{n}{2} \log 2\pi \tag{9}$$

To train the hyperparameters, the locations, X, and elevations, Y, of a small segment of the terrain was provided to the GP. The values of the hyperparameters α and γ were varied over a large range, and the corresponding terrain reconstruction error was calculated from ground truth elevation data. Since the orientation of the world coordinate system should not effect the GP results, the length scales in the two dependent variables are set equal, $\gamma_x = \gamma_y = \gamma$. The values associated with the lowest reconstruction error, $\alpha = 10.0$ and $\gamma = 315.0$, were selected for use in the GP regression in all following results.

E. Simulation Examples

The prototype robotic network has been fielded at several test sites on Mendenhall Glacier near Juneau, AK. However, performing numerical evaluation of the vision system is difficult from the field trial data. An accurate terrain map of the test site locations is unavailable, making assessment of the terrain reconstruction problematic. In order to perform comprehensive numerical analysis of the vision system results, a 3D robotic simulation was developed. This simulation system, which uses Gazebo [30] as its base, has been extended to provide a visually faithful environment including realistic large scale terrain, local scale hazards, and background imagery. Figure 4 shows a visual comparison of the simulated terrain and the real terrain from which it was developed. Additionally, an approach for evaluating the efficacy of the constructed simulation system has also been developed, which makes use of algorithm-specific performance metrics to compare the simulation to the real environment [31]. As the simulation can provide true robot pose information and operates with a known terrain topology, it is an ideal testing platform for localization and terrain reconstruction algorithms.

To test the terrain reconstruction system, one of the Mendenhall Glacier field trial sites was reconstructed within the

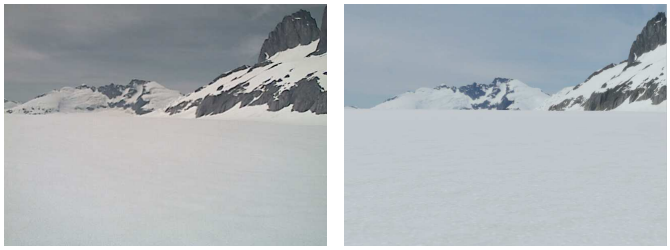

(a) Mendenhall Glacier Field Trial Site (b) Gazebo Simulation

Fig. 4. A visual comparison of (a) the real terrain at a field test site on Mendenhall Glacier, and (b) the resulting simulated terrain.

simulation environment. The control commands from one of the field trial traverses were sent to the simulated rover while the augmented localization algorithm executed against the simulated camera images. During the traverse, any SLAM landmark whose final 1-σ covariance ellipse was no larger than $0.5[m]$ was logged to an external database. During the simulation trial, approximately $50,000$ surface landmarks were sufficiently localized, a vast majority of which occurred very near the rover's path. Because of the proximity of these landmarks, the information they provide is largely redundant. To reduce the number of measurements that must be processed by the GP, only those landmarks that were initialized more than $5[m]$ from the rover's position are used within the reconstruction. This reduces the set to approximately $5,000$ landmarks disbursed over the $600[m]$ x $600[m]$ simulation site.

To compare the performance of the terrain reconstruction system, three different methods have been tested. The first uses a simple linear triangular mesh interpolation method. The Delaunay triangulation [32] is first formed from the SLAM landmark positions. Any query point that falls within the triangulation is estimated using the plane formed by the triangle's vertices. Because query points must fall within a Delaunay triangle to be estimated, this method only produces terrain estimates within the convex hull of the input measurements. Also, there is no obvious mechanism for incorporating measurement uncertainty or *a priori* information into a triangular mesh model.

The second reconstruction incorporates the sparse visual SLAM landmark data into a Gaussian Process model. Unlike the triangular mesh interpolation scheme, the GP model is valid over all of $\mathbb{R}^2$. The mean function used within this reconstruction is a constant derived from the mean elevation of all landmarks used within the reconstruction. The final reconstruction is based on a GP model using the sparse SLAM landmarks as measurements, but also incorporates a non-constant mean function. Raw elevations were extracted from the best available SRTM data products for the simulated test site. These elevation values were used to generate a triangular mesh terrain model capable of interpolating the elevation at any point within the test environment. While the simulated environment is derived from over $200,000$ unique elevations, the raw DEM contained only 64 values. The resulting terrain reconstructions of the simulation environment after the completion of the pre-planned path are shown in Figure 5, with the ground truth elevation map shown in Figure 6 for reference.

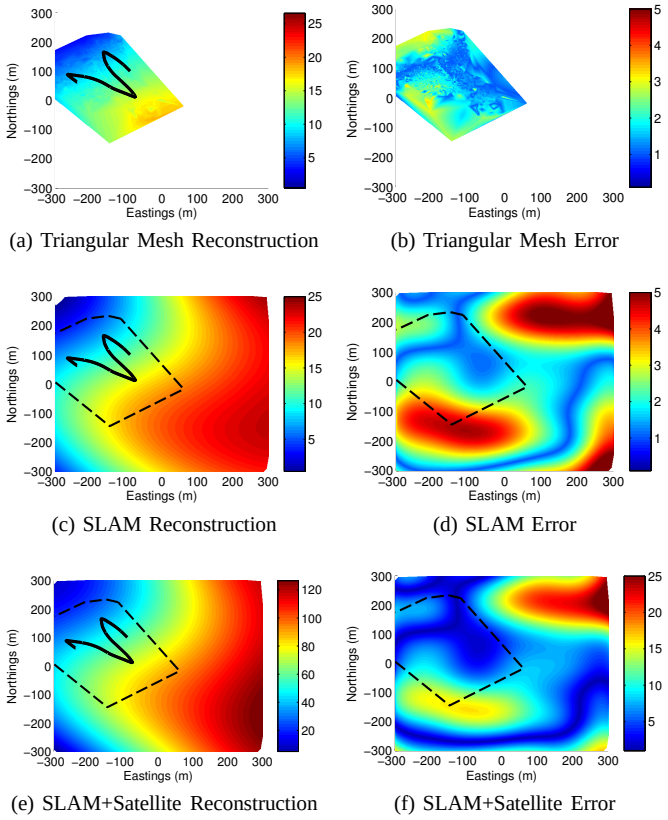

(a) Triangular Mesh Reconstruction (b) Triangular Mesh Error

(c) SLAM Reconstruction (d) SLAM Error

(e) SLAM+Satellite Reconstruction (f) SLAM+Satellite Error

Fig. 5. Terrain reconstructions using data from an example traverse. The rover's path is shown as a solid black line, while the convex hull of landmark points is indicated by a dashed line.

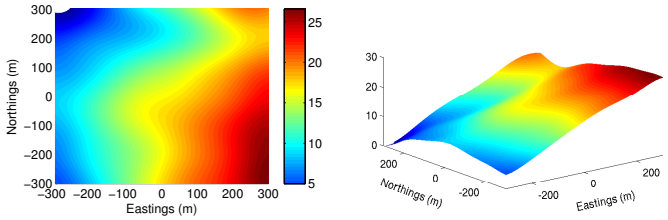

(a) (b)

Fig. 6. The ground truth terrain elevation from the simulated glacial environment.

Perhaps the most striking aspect of the three reconstructions is the limited data provided by the triangular mesh. Only 25.8% of the terrain could be reconstructed after the traverse was completed. In contrast, both GP reconstructions were able to predict the elevation of the entire terrain based on the local observations, even terrain sections that were located behind the rover over the entire traverse. The landmark-only GP reconstruction is able to capture the basic structure of the terrain from the limited data provided, though significant reconstruction errors exist at the terrain boundaries. The landmark plus satellite data GP reconstruction is able to make use of the provided large-scale terrain structure, drastically reducing reconstruction errors at large distances while still adapting locally to the measured environment.

III. Robotic Surveying

In the previous section, a method for generating a terrain reconstruction was presented, motivated by the need to provide an accurate map for path planning algorithms when traveling in unknown or dynamic environments. However, the terrain reconstruction itself may be viewed as a valuable scientific data product. Estimating the annual glacial melt in the Arctic, for example, is one such motivation for accurate terrain reconstruction (other motivations include mineral prospecting or chemical concentration monitoring in soil [33], [34]). Currently, remote sensing methods lack the sensing instrumentation necessary to collect important spatial detail in the shape and recession of portions of the glaciers of interest to Earth scientists. Traditionally, scientists rely on *in situ* methods for collecting this detail. The drawbacks of current methods include lack of safety for human scientists, dearth of moderate coverage, and high cost [35].

To ensure the reconstructed terrain model results in a valid scientific product, we need to ensure that the terrain complies with topographic mapping standards. While the method GP reconstruction method discussed previously showed preliminary results based on terrain points gathered opportunistically, in order to ensure compliance with mapping requirements, we require that survey paths are planned based on a desired maximum reconstruction error. In traditional robot surveying projects, typical navigation patterns follow a lawnmower structure [36], [37]. On the other hand, in the scientific realm, samples are extracted based on investigation of the features needed to properly estimate change of environmental phenomena [38]. As such, we need to employ a methodology that defines a robot navigation pattern based on a sampling methodology that properly covers the space of changes in environmental characteristics. In addition, our methods must be validated based on actual mapping requirements set forth by the photogrammetric and cartographic professions.

A. Robot Navigation and Science-centric Coverage

In robotics, the coverage problem is typically defined by the requirement to maximize the total area covered by a robotic system [39]. On the other hand, in the scientific community, coverage is defined based on properly measuring the space of environmental phenomena [38]. In robotics, many successful surveying techniques [37], [40], [41] focus on performing a raster scan ($i.e.$, lawnmower) by designating evenly distributed, linear traverses across an area of interest in order to address the coverage problem. By designating swatch width, this type of navigation pattern enables the system to retrieve an even distribution of samples. Unfortunately, this static approach is usually implemented for the purposes of search [42] and thus does not adapt to environmental phenomena measured in-situ during the traverse. As such, our objectives are to both define a navigation pattern that sufficiently samples the space of environmental phenomena but also define metrics as it relates to collecting information most useful to the scientist.

To achieve the first objective, we employ an augmentation to the lawnmower navigation pattern using a method called

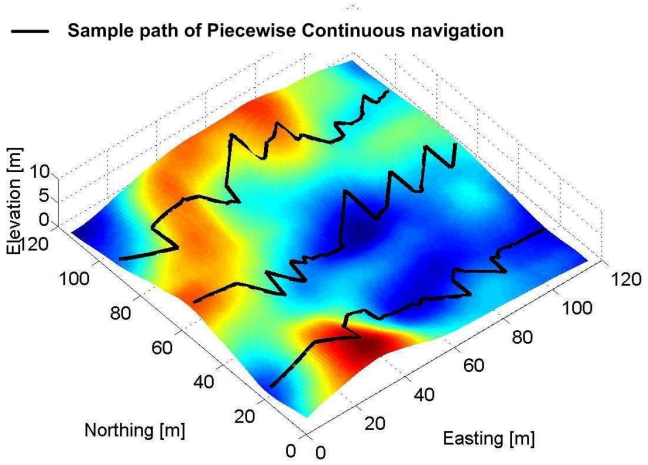

Fig. 7. Example terrain exhibiting slowly-varying, continuous elevation trends superimposed with a sample Piecewise Continuous navigation path.

piecewise-continuous [43] in which the sampling path deviates around a linear reference swath based on sensed phenomena within the terrain. The specific heuristic applied in this work is a policy defined by a switching mechanism, alternating between gradient-ascent and gradient-descent rules for changing direction based on sensed features within the terrain (Equation (10)).

$$f_{s+1}(q) = \begin{cases} min(\vec{\nabla} f_s(q)) & \text{if } flag = 0 \\ max(\vec{\nabla} f_s(q)) & \text{if } flag = 1 \end{cases} \quad (10)$$

In Equation (10), the function, $f_{s+1}(q)$ represents the next state of the navigating agent, $f_s(q)$ represents the agent's current state, s is an incremental tracker of the number of samples, and q is the specific location of the agent. The switching feature, mentioned earlier, is represented by $flag$, which is randomly toggled during navigation for the purpose of influencing spatial diversity in the path achieved by the agent.

We have shown that this type of methodology correlates closely to processes found in the sampling and surveying literature [38] and outperforms traditional lawnmower for continuous, slowly-varying, terrains of interest (Figure 7) [43].

With respect to the second objective, we must define metrics that correlate robot traverse to information most useful to the scientist. Typical navigation work in the robotics community defines coverage as the ratio of some total measure of Euclidean distance traveled by a robotic agent, D_S, to some maximum distance, D_T. It is generally accepted that as D_S approaches D_T, the goal of achieving complete coverage of an area is inferred. Measuring coverage in this way places attention on the agent and its performance rather than the search space and the quality of samples collected during navigation. If, instead, the search space is discretized to quantify the total number of samples that can be collected within the area of interest, a more useful definition of coverage for science sampling can be defined.

We define a type of coverage relative to the cummulative sum of distances from all possible sample locations to the center of the area of interest. Percent science-centric coverage

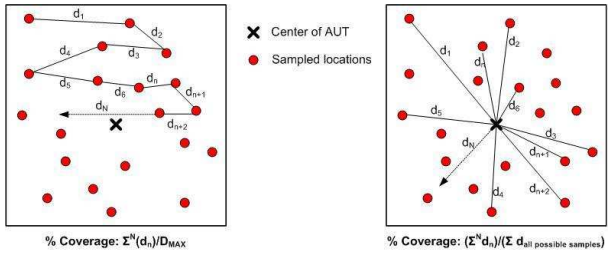

Fig. 8. Difference in percent coverage definition of an area of interest: robot-centric (left), science-centric (right).

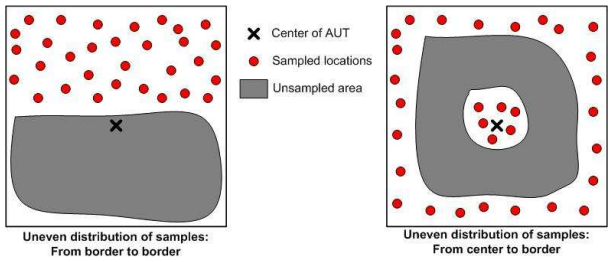

Fig. 9. Examples of misleading sample distributions across an area of interest.

(SCC) is the ratio of T_M, the sum of relative distances between actual samples, (x_m, y_m), and a reference location within the search space, (X_{ref}, Y_{ref}), to T_S, the sum of relative distances between all possible samples, (x_s, y_s), and that same reference location (Equation (11)).

$$\% \text{ SCC} = \frac{T_M}{T_S} = \frac{\sum_{m=1}^{M} \|(x_m, y_m) - (X_{ref}, Y_{ref})\|}{\sum_{s=1}^{S} \|(x_s, y_s) - (X_{ref}, Y_{ref})\|} \quad (11)$$

For each level of desired coverage designated by a scientist, we assess a measure of percent SCC, attaching with it the success of the sample set (measured in the form of root mean squared error). Defining distances relative to a specific point, $i.e.$ (X_{ref}, Y_{ref}), prioritizes the importance of the samples collected over that of the agent and provides each sample with a relative meaning (Figure 8).

To ensure this definition of percent SCC is used appropriately to evaluate future navigation schemes, spatially-relevant characteristics of the samples collected should also be defined. Specifically, there needs to be a way of evaluating how centered and distributed a given sample set is throughout the area of interest.

B. Centeredness and Distribution

Symmetry and distribution of samples collected by a navigation scheme are valuable to an Earth scientist when an accurate representation of changes in measured phenomena are desired. Following a science-related survey, the projected statistics of the samples collected may be reported as 50 percent, while the sample distribution is actually asymmetrically placed across the area of interest. Similarly, the center of mass (CoM) of a collected set of samples may be placed close to the center of the testing area, but only truly reflect a clustering at the border and/or very center of the area of interest (Figure 9).

We identify α and β as the complimentary tools to accompany our assessment of coverage. Here, α represents a measure of the "centeredness" of a set of samples of size M, while β represents the "distributedness" of samples between each reference swath.

To calculate α, we determine the planimetric center of mass (CoM) of a particular sample set, found in (12), where (x_m, y_m) is the location of each sample and M is the total number of samples collected.

$$[X_{CoM}, Y_{CoM}] = \frac{\sum_{k=1}^{M} (x_m, y_m)}{M}, \quad (12)$$

Using CoM, we define α (13).

$$\alpha = \frac{\|(X_{CoM}, Y_{CoM}) - (X_{ref}, Y_{ref})\|}{D_{Max}}, \quad (13)$$

In (13), D_{Max} is the maximum possible distance between the sample set's center of mass and (X_{ref}, Y_{ref}), while (X_{ref}, Y_{ref}) is the reference location from which the actual sample set's center of mass is measured. To effectively assess how well our samples, resulting from our navigation, are distributed within the search space, we must emphasize the costly nature of diverting from a linear path. For a series of M samples, if we consider a particular sample at location (x_m, y_m), a subsequent sample at location (x_{m+1}, y_{m+1}), and a reference swath around which these samples are collected, y_{swath}, then we can define β (16).

$$\beta_a = \frac{\sum_{m=1}^{M} |y_m - y_{swath}|}{M} \quad (14)$$

$$\beta_b = \frac{\sum_{m=1}^{(M-1)} |y_m - y_{m+1}|}{(M-1)}, \text{ for } |y_m - y_{m+1}| \geq 1 \quad (15)$$

$$\beta = \frac{\beta_a}{\beta_b} \quad (16)$$

We define β as a ratio of the average distance away from the reference swath to the average change in distance away from that same reference. While β_a provides a measure of how dispersed around its reference, y_{swath}, a sample set is, this dispersion value is penalized based on how distant successive samples are from one another, a measurement designated as β_b. Using β_b allows us to quantify the importance of achieving sequential samples concurrent with the placement of those samples reaching areas of the search space beyond the designated reference. Given these metrics, we now have additional ways of evaluating the quality of coverage provided by a particular navigation pattern.

C. Mapping Accuracy Standards

Lastly, we must ensure that the map regeneration we produce meets a predefined error maximum set forth by those most interested in the science product. Although desired map accuracies can vary, we refer to the accepted accuracy standards employed by professionals in the cartographic and photogrammetry fields [44]. In the case of map elevation, the american society for photogrammetry and remote sensing

TABLE I
ASPRS CLASS 1 MAP ACCURACY STANDARDS (VERTICAL).

Horizontal Contour Interval [m]	Vertical ASPRS-RMS error [m]
0.3048 (1 [ft])	0.0508
0.6096 (2 [ft])	0.1016
0.9144 (3 [ft])	0.1524

TABLE II
ASPRS CLASS 2 MAP ACCURACY STANDARDS (VERTICAL).

Horizontal Contour Interval [m]	Vertical ASPRS-RMS error [m]
0.6096 (2 [ft])	0.1016
1.2192 (4 [ft])	0.2032
1.8288 (6 [ft])	0.3048

(ASPRS) standard quantifies vertical root mean squared error specifications that dictate how a mapping product may be classified (Tables I-III).

One motivation behind the ASPRS standard was set to clarify the accuracy of map data when represented as a 2D contour plot, with each contour line representing a specific elevation. The tables presented earlier clarify the level of vertical elevation accuracy based on specific horizontal separation between successive contour lines. When seeking a map product in the form of a 2D contour map with contour separation equal to K [m], the average map error estimated must be no greater than K/6 [m] or one-sixth the contour separation. Thus, a desired contour separation of 3 [ft] (0.9144 [m]) requires an average error no greater than 0.1524 [m]. According to ASPRS, there exist three distinct classes of map accuracies based on contour line separations ranging from 1 [ft] to 9 [ft]. The specific maximum allowable error varies depending on the needs of the scientist, but once a value is agreed upon, it provides a benchmark for validating our results. Figure 10 shows the evaluation of these navigation patterns against typical terrains, such as the one shown in Figure 7, relative to accepted mapping standards.

IV. RESULTS

We evaluate the performance of our vision system and surveying methods based on the successful reconstruction of our environment. As a test, the system has been tasked to create a Class 3 elevation map. In this context, a reconstruction is considered successful if the final elevation model meets the minimum criteria for the map type selected. This implies a maximum terrain reconstruction error of $0.46[m]$, as described

TABLE III
ASPRS CLASS 3 MAP ACCURACY STANDARDS (VERTICAL).

Horizontal Contour Interval [m]	Vertical ASPRS-RMS error [m]
0.9144 (3 [ft])	0.1524
1.8288 (6 [ft])	0.3048
2.7432 (9 [ft])	0.4572

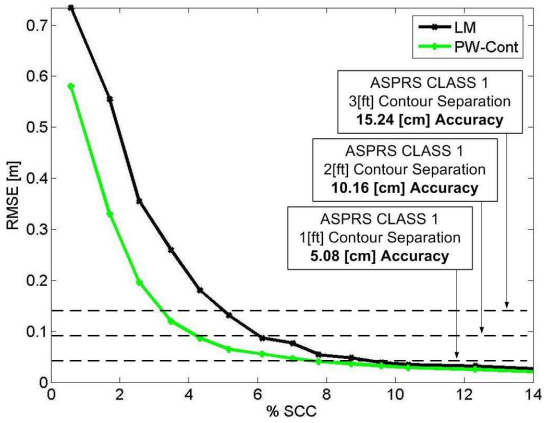

Fig. 10. ASPRS standard annotation of average RMS error based on data collected by specific navigation patterns across 100 randomly generated DEMs.

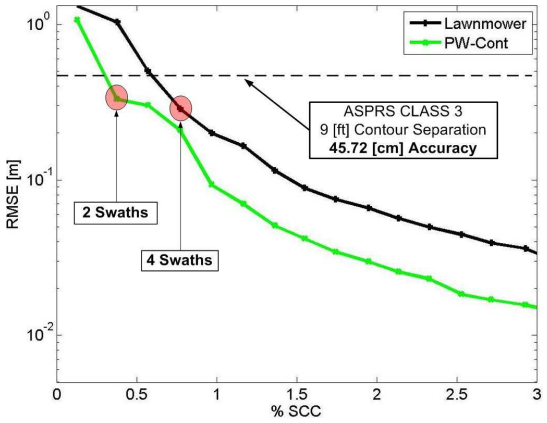

Fig. 11. Average reconstruction error annotated with maximum error requirement for Class 3 map for each navigation pattern.

in Table III. The area to be surveyed is a simulation of a $600[m]$ x $600[m]$ field test site on Mendenhall Glacier. Using satellite elevation data, the maximum terrain variation over this area is found to be approximately $25[m]$. However, this is merely an estimate of the terrain variation, as each satellite measurement is actually an average elevation over a large area. Using this maximum terrain variation estimate, a set of random terrains were simulated numerically, using the procedure outlined in Section III. Figure 11 shows the average reconstruction error of the random environments when surveyed by different path planning approaches. The maximum error requirement for the Class 3 map is superimposed on the results. From this graph, the minimum number of surveying swaths for each algorithm may be extracted (four swaths for traditional lawnmower and two swaths for piecewise continuous).

The simulation system described in Section II has again been employed to validate the surveying path predictions. The simulated rover is placed at a starting point within the simulation, which is assumed to be a known location. The rover is then tasked to drive through a series waypoints calculated from the selected surveying pattern. During these traverses, the vision-augmented localization system maps the location of any visually distinct texture points encountered. These 3D surface estimates are used as inputs to the Gaussian Process

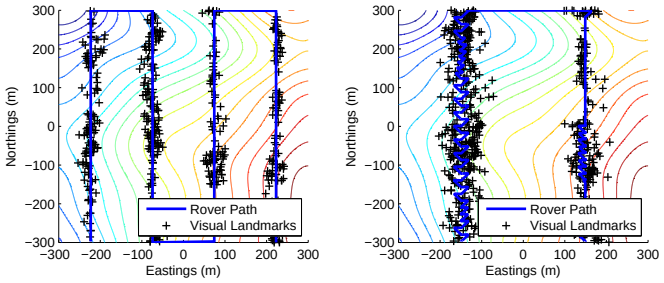

Fig. 12. The executed rover paths and an indication of the spacial distribution of the visual landmark for (a) the lawnmower surveying strategy and (b) the piecewise continuous surveying strategy.

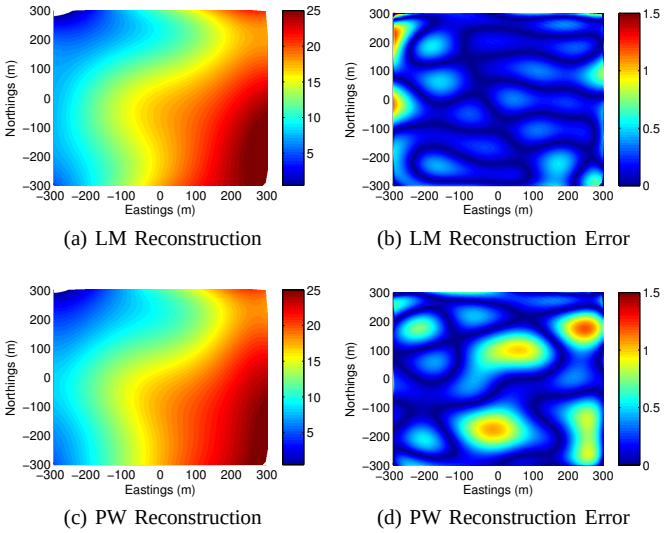

Fig. 13. Terrain reconstructions and reconstruction errors using data from (a-b) the lawnmower surveying strategy and (c-d) the piecewise continuous surveying strategy.

(GP) terrain model. These surface points are analogous to GPS survey information, with the exception that the sampled locations are controlled by the visual surface appearance rather than a planned sampling scheme. In the case of the Piecewise Linear survey algorithm, the path actually adapts in response to the surface conditions. These decisions are based on the pose estimate of the rover, as intermediate terrain reconstructions are not available to the rover during the surveying process. Figure 12 shows the executed rover paths for each surveying strategy, and an indication of the spacial distribution of the visual landmarks.

Finally, a terrain reconstruction is performed for each surveying algorithm using the GP framework described in Section II (Figure 13). Based upon our simulated prediction of the number of swaths required to achieve the maximum ASPRS mapping standard error for a Class 3 map (0.4572 [m]), our system achieves RMS error of 0.2827 [m] and 0.3323 [m], when navigating according to the traditional Lawnmower pattern and Piecewise Continuous navigation respectively.

The outcome of our testing highlights two salient aspects of our work. The first point is the performance of our vision system as a sensor to generate useful science information for terrain reconstruction despite its inherent error-prone measurements. The information extracted from Figure 11 used to dictate the minimum number of traverses to achieve maximum error for each navigation strategy was obtained presuming a perfect sensor. In accordance with this prediction from simulation, we are pleased with the RMS error obtained with visual SLAM sensing. Yielding a difference between predicted and actual of 0.0358 [m] (12.43%) when navigating according to the traditional Lawnmower pattern and 0.0733 [m] (22%) when adhering to the Piecewise Continuous navigation path, both absolute error values meet the desired Class 3 maximum error limit (Table III).

The second noticeable item is the importance of the terrain's spatial complexity when selecting one navigation strategy over another. The simple downward-slope feature of our testing terrain reduces the need for spatially diverse paths, where as a test area more analogous to the one shown in Figure 7 typically demands more flexibility in changing navigation directions given the increased presence of hills and valleys.

V. Conclusions

In this paper, we have discussed a methodology for terrain reconstruction of glacier environments based on observed phenomena during a robot traverse. The principle take-away from our work highlights the significance of augmenting intelligent navigation schemes with environmentally-relevant sensing capabilities to comply with desired scientific objectives. Although our focus in this paper was on terrain elevation as the measured phenomenon, the navigation strategies presented herein remain valid even in the event that the environmental phenomena shift domains, *i.e.* soil moisture versus elevation data. Future work will thus involve applying our approach to observing these alternative phenomena, as well as deploying multiple agents in this field. These field campaigns range from accurately monitoring chemical plumes to providing timely spatial characterization of radiation distribution across an area. We believe that by coupling robotics with science-based objectives such as these, major life-preserving opportunities could continue to be addressed by the robotics community.

Acknowledgments

This work was supported by the National Aeronautics and Space Administration under the Earth Science and Technology Office, Applied Information Systems Technology Program. The authors would also like to express their gratitude to Dr. Matt Heavner, Research Scientist, Los Alamos National Lab (formerly Associate Professor of Physics, University of Alaska Southeast), for providing logistical support and his expertise in glacial field work.

References

[1] J. Curry, J. Schramm, and E. Ebert, "Sea ice-albedo climate feedback mechanism," *Journal of Climate*, vol. 8, no. 2, pp. 240–247, 1995.

[2] M. Serreze and R. Barry, *The Arctic climate system*. Cambridge Univ Press, 2005.

[3] J. Stroeve, J. E. Box, F. Gao, S. Liang, A. Nolin, and C. Schaaf, "Accuracy assessment of the modis 16-day albedo product for snow: comparisons with greenland in situ measurements," *Remote Sensing of Environment*, vol. 94, pp. 46 – 60, 2005.

[4] V. B. Spikes and G. S. Hamilton, "Glas calibration-validation sites established on the west antarctic ice sheet," in *International Symposium on Remote Sensing of Environment*, Honolulu, Hawaii, 2003.

[5] S. Williams, A. Viguria, and A. M. Howard, "A robotic mobile sensor network for achieving scientific measurements in challenging environments," in *Proceedings of the Earth Science Technology Conference*, Washington, DC, June 2008.

[6] E. Dijkstra, "A note on two problems in connexion with graphs," *Numerische mathematik*, vol. 1, no. 1, pp. 269–271, 1959.

[7] S. LaValle, "Rapidly-exploring random trees: A new tool for path planning," TR 98-11, Computer Science Dept., Iowa State University, Tech. Rep., 1998.

[8] F. Paul and W. Haeberli, "Spatial variability of glacier elevation changes in the swiss alps obtained from two digital elevation models," *Geophysical Research Letters*, vol. 35, 2008.

[9] M. Miller and M. Pelto, "Mass balance measurements on the lemon creek glacier, juneau icefield, alaska 1953–1998," *Geografiska Annaler: Series A, Physical Geography*, vol. 81, no. 4, pp. 671–681, 1999.

[10] D. Apostolopoulos, M. D. Wagner, B. Shamah, L. Pedersen, K. Shillcutt, and W. R. L. Whittaker, "Technology and field demonstration of robotic search for antarctic meteorites," *International Journal of Robotics Research*, vol. 19, no. 11, p. 1015, Dec 2000.

[11] L. Pedersen, D. Wettergreen, D. Apostolopoulos, C. McKay, M. DiGoia, S. Heys, J. Teza, M. Wagner, and K. A. Ali, "Rover design for polar astrobiological exploration," in *Proceedings of the 8th International Symposium on Artificial Intelligence, Robotics and Automation in Space, i-SAIRAS*, 2005.

[12] E. L. Akers, H. P. Harmon, R. S. Stansbury, and A. Agah, "Design, fabrication, and evaluation of a mobile robot for polar environments," in *Proceedings of the IEEE International Geoscience and Remote Sensing Symposium, IGARSS*, vol. 1, Anchorage, Alaska, Sept 2004.

[13] C. M. Gifford, E. L. Akers, R. S. Stansbury, and A. Agah, *Mobile Robots for Polar Remote Sensing*. Springer Publishing Company, Incorporated, 2009, pp. 1–22.

[14] S. Goldberg, M. Maimone, L. Matthies, I. Syst, and C. Northridge, "Stereo vision and rover navigation software for planetary exploration," in *Proceedings of the IEEE Aerospace Conference*, vol. 5, Big Sky, MT, March 2002.

[15] M. Montemerlo, S. Thrun, H. Dahlkamp, D. Stavens, and S. Strohband, "Winning the DARPA grand challenge with an AI robot," in *Proceedings of the National Conference on Artificial Intelligence*, vol. 21, Boston, MA, July 2006, p. 982.

[16] C. Harris and M. Stephens, "A combined corner and edge detector," in *Proceedings of the Alvey vision conference*, Manchester, UK, 1988, pp. 147–151.

[17] D. Lowe, "Object recognition from local scale-invariant features," in *Proceedings of the IEEE International Conference on Computer Vision, ICCV*, vol. 2, 1999, pp. 1150–1157.

[18] S. Williams and A. Howard, "Developing monocular visual pose estimation for arctic environments," *Journal of Field Robotics*, vol. 27, no. 2, pp. 145–157, 2010.

[19] S. Williams, L. Parker, and A. Howard, "Calibration and validation of earth-observing sensors using deployable surface-based sensor networks," *IEEE Journal of Selected Topics in Applied Earth Observations and Remote Sensing*, vol. 3, no. 4, pp. 427–432, 2010.

[20] S. Williams, M. Hurst, and A. Howard, "Development of a mobile arctic sensor node for earth-science data collection applications," in *Proceedings of the American Institute of Aeronautics and Astronautics, Infotech@Aerospace*, Atlanta, GA, April 2010.

[21] S. Williams and A. M. Howard, "A single camera terrain slope estimation technique for natural arctic environments," in *Proceedings of the IEEE International Conference on Robotics and Automation, ICRA*, Pasadena, CA, May 2008, pp. 2729–2734.

[22] ——, "Towards visual arctic terrain assessment," in *Proceedings of the International Conference on Field and Service Robotics, FSR*, Cambridge, MA, July 2009.

[23] T. Farr *et al.*, "The shuttle radar topography mission," *Reviews of Geophysics*, vol. 45, no. 2, 2007.

[24] H. Zwally, B. Schutz, W. Abdalati *et al.*, "ICESat's laser measurements of polar ice, atmosphere, ocean, and land," *Journal of Geodynamics*, vol. 34, no. 3-4, pp. 405–445, 2002.

[25] C. Rasmussen and C. Williams, "Gaussian processes for machine learning," 2006.

[26] R. Von Mises, *Mathematical Theory of Probability and Statistics*. New York, NY: Academic Press Inc., 1964, ch. 9.3, pp. 427–430.

[27] W. A. Fuller, *Measurement Error Models*. Hoboken, NJ: John Wiley & Sons, Inc., 1987, ch. 4, pp. 292–360.

[28] USGS, "http://egsc.usgs.gov/isb/pubs/factsheets/fs17199.html."

[29] C. Rasmussen, "Gaussian processes in machine learning," *Advanced Lectures on Machine Learning*, pp. 63–71, 2004.

[30] B. P. Gerkey, R. T. Vaughan, and A. Howard, "The Player/Stage project: Tools for multi-robot and distributed sensor systems," in *Proceedings of the International Conference on Advanced Robotics, ICAR*, Coimbra, Portugal, July 2003, pp. 317–323.

[31] S. Williams, S. Remy, and A. Howard, "3D simulations for testing and validating robotic-driven applications for exploring lunar poles," in *Proceedings of the American Institute of Aeronautics and Astronautics, Infotech@Aerospace*, Atlanta, GA, April 2010.

[32] M. De Berg, O. Cheong, M. Van Kreveld, and M. Overmars, *Computational geometry: algorithms and applications*. New York, NY: Springer-Verlag Inc., 2008, ch. 9, pp. 191–218.

[33] J. Meersmans, F. D. Ridder, F. Canters, S. D. Baets, and M. V. Molle, "A multiple regression approach to assess the spatial distribution of soil organic carbon (soc) at the regional scale (flanders, belgium)," *Geoderoma*, no. 143, pp. 1–13, 2008.

[34] M. Billa, D. Cassard, A. L. W. Lips, V. Bouchot, B. Tourliere, G. Stein, and L. Guillou-Frottier, "Predicting gold-rich epithermal and porphyry systems in the central andes with a continental-scale metallogenic gis," *Ore Geology Reviews*, vol. 25, pp. 39–67, 2004.

[35] L. T. Parker and A. M. Howard, "Real-time robotic surveying for unexplored arctic terrain," in *NASA Earth Science Technology Forum*, June 22 – 24 2010.

[36] E. Tunstel, J. Dolan, T. W. Fong, and D. Schreckenghost, "Mobile robotic surveying performance for planetary surface site characterization," in *Performance Evaluation and Benchmarking of Intelligent Systems*, E. Tunstel and E. Messina, Eds. Springer, August 2009.

[37] B. S. Bourgeois, D. L. Brandon, J. J. Cheramie, and J. Gravley, "Efficient hydrographic survey planning using an environmentally adaptive approach," in *DoD Technical Report*, Stennis Space Center, MS, 2006.

[38] R. Webster and M. A. Oliver, *Geostatistics for Environmental Scientists*. John Wiley & Sons Publishing, 2003.

[39] "Command control for many-robot systems."

[40] R. Dechter and J. Pearl, "Generalized best-first search strategies and the optimality of a*," *J. ACM*, vol. 32, pp. 505–536, July 1985.

[41] A. Stentz, "The focussed d* algorithm for real-time replanning," in *In Proceedings of the International Joint Conference on Artificial Intelligence*, 1995, pp. 1652–1659.

[42] R. R. Hashemi, L. Jin, G. T. Anderson, E. Wilson, and M. R. Clark, "A comparison of search patterns for cooperative robots operating in remote environment," in *IEEE Int. Conference on Information Technology: Coding and Computing*, Las Vegas, NV, 2001.

[43] L. T. Parker and A. M. Howard, "Adaptive robot navigation protocol for estimating variable terrain elevation data," in *IEEE Int. Conference on Systems, Man, and Cybernetics (accepted)*, Anchorage, AK, October 2011.

[44] *Geospatial Positioning Accuracy Standards Part 3: National Standard for Spatial Data Accuracy*, Fgdc-std-007.3-1998 ed., Subcommittee for Base Cartographic Data, Fedreal Geographic Data Committee, 1998.

Stephen Williams School of Electrical and Computer Engineering, Georgia Institute of Technology, Atlanta, GA 3033, USA. E-mail: `swilliams8@gatech.edu`.

Lonnie T. Parker School of Electrical and Computer Engineering, Georgia Institute of Technology, Atlanta, GA 3033, USA. E-mail: `lonnie@gatech.edu`.

Ayanna M. Howard School of Electrical and Computer Engineering, Georgia Institute of Technology, Atlanta, GA 3033, USA. E-mail: `ayanna.howard@ece.gatech.edu`.